Received: 13 June 2022 | Revised: 20 January 2023 | Accepted: 24 January 2023

DOI: 10.1111/cas.15738

Cancer Science WILEY

ORIGINAL ARTICLE

IFN-γ–STAT1-mediated NK2R expression is involved in the induction of antitumor effector CD8$^+$ T cells in vivo

Weidong Shen[1] | Xiangdong Wang[1] | Huihui Xiang[1] | Shunsuke Shichi[1,2] | Hiroki Nakamoto[1,2] | Saori Kimura[1,2] | Ko Sugiyama[1,2] | Akinobu Taketomi[2] | Hidemitsu Kitamura[1]

[1]Division of Functional Immunology, Section of Disease Control, Institute for Genetic Medicine, Hokkaido University, Sapporo, Japan

[2]Department of Gastroenterological Surgery I, Hokkaido University Graduate School of Medicine, Sapporo, Japan

Correspondence
Hidemitsu Kitamura, Division of Functional Immunology, Section of Disease Control, Institute for Genetic Medicine, Hokkaido University, Kita-15, Nishi-7, Kita-ku, Sapporo 060-0815, Japan.
Email: kitamura@igm.hokudai.ac.jp

Funding information
Japan Society for the Promotion of Science, Grant/Award Number: 22K07017; Japan Agency for Medical Research and Development, Grant/Award Number: 22fk0310524h0001; Hokkaido University

Abstract

The induction of antitumor effector T cells in the tumor microenvironment is a crucial event for cancer immunotherapy. Neurokinin receptor 2 (NK2R), a G protein-coupled receptor for neurokinin A (NKA), regulates diverse physiological functions. However, the precise role of NKA–NK2R signaling in antitumor immunity is unclear. Here, we found that an IFN-γ–STAT1 cascade augmented NK2R expression in CD8$^+$ T cells, and NK2R-mediated NKA signaling was involved in inducing antitumor effector T cells in vivo. The administration of a synthetic analog of double-stranded RNA, polyinosinic–polycytidylic acid (poly I:C), into a liver cancer mouse model induced type I and type II IFNs and significantly suppressed the tumorigenesis of Hepa1-6 liver cancer cells in a STAT1-dependent manner. The reduction in tumor growth was diminished by the depletion of CD8$^+$ T cells. IFN-γ stimulation significantly induced NK2R and tachykinin precursor 1 (encodes NKA) gene expression in CD8$^+$ T cells. NKA stimulation combined with anti-CD3 monoclonal antibody (mAb) treatment significantly augmented IFN-γ and granzyme B production by CD8$^+$ T cells compared with the anti-CD3 mAb alone in vitro. ERK1/2 phosphorylation and IκBα degradation in activated CD8$^+$ T cells were suppressed under NK2R deficiency. Finally, we confirmed that tumor growth was significantly increased in NK2R-deficient mice compared with that in wild-type mice, and the antitumor effects of poly I:C were abolished by NK2R absence. These findings suggest that IFN-γ–STAT1-mediated NK2R expression is involved in the induction of antitumor effector T cells in the tumor microenvironment, which contributes to the suppression of cancer cell tumorigenesis in vivo. In this study, we revealed that IFN-γ–STAT1-mediated NK2R expression is involved in the induction of antitumor effector CD8$^+$ T cells in the tumor microenvironment, which contributes to suppressing the tumorigenesis of liver cancer cells in vivo.

Abbreviations: IFN, interferon; IκBα, nuclear factor of kappa light polypeptide gene enhancer in B-cells inhibitor, alpha; MFI, mean fluorescence intensity; NK2R, neurokinin receptor 2; NKA, neurokinin A; OVA, ovalbumin; Poly I:C, polyinosinic–polycytidylic acid; STAT, signal transducer and activator of transcription; TCR, T cell receptor.

KEYWORDS
effector CD8+ T cells, hepatocellular carcinoma, IFN-γ, NK2R, STAT1

1 | INTRODUCTION

In recent years, cancer immunotherapies, such as immune checkpoint inhibition and adoptive transfer of chimeric antigen receptor T cells, have been developed and contributed to improving the prognosis of cancer patients.[1] Generally, the induction and activation of tumor-specific killer T cells and their introduction into the tumor microenvironment are the most important issues for effective cancer immunotherapy.[2] Many papers have reported that cancer patients with reduced killer T cells in the tumor microenvironment, so-called "cold tumors," show decreased antitumor effects of cancer immunotherapy.[3] Therefore, to improve the effectiveness of cancer immunotherapy, various methods, such as the removal of immunosuppressive cells and administration of immune adjuvants, have been attempted to introduce effector T cells into the tumor microenvironment.

Excitatory transmitters, such as substance P and NKA belonging to the tachykinin family, are widely distributed within the central and peripheral nervous systems. Although tachykinins were initially considered neurotransmitters, several articles have reported the expression of their receptors NK1R and NK2R in nonneural tissues, including endothelial cells, fibroblasts, smooth muscle cells, inflammatory cells, and various types of cancer cells, suggesting that tachykinins function between the nervous system and other organs, including tumor tissues.[4–7]

A previous study has reported that IFN-γ or lipopolysaccharide stimulation induced NKA and NK2R expression in murine dendritic cells in a STAT1-dependent manner, and the enhanced NK2R expression-mediated NKA signaling augmented the induction of ovalbumin antigen-specific CD4+ T cells and CD8+ T cells.[8] Furthermore, we revealed that IFN-α, IFN-β, or polyinosinic–polycytidylic acid (poly I:C) treatment induced NK1R and NK2R expression in human monocyte-derived dendritic cells in a STAT1-dependent manner, and NK1R/NK2R-mediated neuropeptide signaling contributed to the activation of allergen-specific T cells, which might be involved in the pathology of severe asthma.[9] In our recent research, we revealed that IFN-α/β-mediated NK2R expression was related to the malignancy of colon cancer cells.[10] However, the precise effects of IFN–STAT1-mediated NKA–NK2R signaling on the induction of antitumor effector cells in the tumor microenvironment are unclear.

Hepatocellular carcinoma (HCC), a common liver cancer worldwide, has a high recurrence rate after surgery and is the second-leading cause of cancer-related deaths globally.[11,12] The elucidation of the precise mechanisms involved is required for the development of more effective treatments for patients with HCC. Recently, several excellent therapeutic effects of immune checkpoint inhibitors in the standard treatment of HCC patients have been reported.[13,14] The activation of JAK/STAT1 signaling inhibits the proliferation of liver cancers and enhances antitumor effects.[15,16] Previous studies have demonstrated that STAT1 deficiency in the tumor-bearing host augmented the tumorigenesis of HCC by decreasing the introduction of antitumor effector cells.[17–19] Our recent study revealed the excellent antitumor effects of the combined administration of an anti-programmed death-ligand 1 (PD-L1) antibody with diacylglycerol kinase alpha (DGKα) inhibition, which is a promising cancer therapeutic target.[20] Furthermore, in this study, we confirmed that IFN-γ-producing antitumor effector T cells are efficiently introduced into the tumor microenvironment.

In the present study, we found that IFN-γ stimulation induced NK2R gene expression in CD8+ T cells in a STAT1-dependent manner and confirmed that NK2R-deficient CD8+ T cells exhibited decreased production of IFN-γ and granzyme B. Furthermore, we found that tumor growth was significantly increased and that the infiltration of CD8+ T cells in tumor tissues was reduced under NK2R-deficient conditions. In this paper, we report that the IFN–STAT–NK2R axis provides a promising target in the induction of antitumor immunity in tumor microenvironments.

2 | MATERIALS AND METHODS

2.1 | Antibodies, cytokines, and chemicals

Fluorescent dye-conjugated anti-CD45 (30-F11), anti-CD4 (GK1.5), anti-CD8 (53–6.7), anti-NK1.1 (PK136), anti-CD11c (HL3), anti-IFN-γ (XMG1.2), anti-granzyme B (QA16A02), anti-CD62L (MEL-14), and anti-CD44 (IM7) monoclonal antibodies (mAbs) were purchased from BioLegend or BD Biosciences. Purified anti-mouse CD3e (145-2C11) and purified anti-mouse CD28 (37.51) mAbs were obtained from BioLegend or BD Biosciences. mAbs for CD8 depletion (clone 53.6.7) and NK1.1 depletion (clone PK136) were purchased from Bio X Cell. Microbeads conjugated with anti-CD8 (53–6.7) mAb were purchased from BD Biosciences. Recombinant murine IFN-γ was purchased from PeproTech EC. 7-AAD Viability Dye was purchased from BECKMAN COULTER. Rabbit CD4 (D7D2Z) (#25229) and CD8α (D4W2Z) (#98941) mAbs for immunohistochemistry were obtained from Cell Signaling Technology. Rabbit mAbs for western blotting, including p44/42 mitogen-activated protein kinase (MAPK) (Erk1/2) (137F5) (#4695), phospho-p44/42 MAPK (Erk1/2) (Thr202/Tyr204) (D13.14.4E) (#4370), IκBα (C-21) (sc371), and horseradish peroxidase (HRP)-conjugated anti-rabbit IgG (#7074), were obtained from Cell Signaling Technology. The mouse α-tubulin (DM1A) (115M4796) mAb and HRP-conjugated anti-mouse IgG (ab97023) for western blotting were obtained from Abcam. Poly I:C was purchased from InvivoGen. ISOGEN RNA extraction reagent was purchased from Nippon Gene. The NK2R selective agonist (neurokinin A) was purchased from Peptide Institute, Inc.

2.2 | Mice and cell lines

Wild-type C57BL/6 and BALB/c mice were obtained from Charles River Japan (Kanagawa, Japan). STAT1-deficient (*Stat1*$^{-/-}$) mice were kindly provided by Dr. R. Schreiber (Washington University School of Medicine). Sperm from C57BL/6-background NK2R-deficient (*Tacr2*$^{-/-}$) mice was obtained from the KOMP Repository, University of California (Davis, CA, USA), and in vitro fertilization was performed at the Central Institute for Experimental Animals (Kawasaki, Kanagawa, Japan). All mice were maintained in specific pathogen-free conditions and used at 8–12 weeks of age. All mouse experiments were approved by the Animal Ethics Committee of Hokkaido University (19-0036, 21-0026) and conducted in accordance with the recommendations in the Guide for the Care and Use of Laboratory Animals of the University. The murine liver cancer cell line Hepa1-6 (ATCC® CRL-1830™) was obtained from the ATTC (Manassas, VA, USA). The murine colon cancer cell line CT26 (CRL-2638) and OVA-expressing T lymphoblasts EG7-OVA (CRL-2113) were obtained from the ATTC (VA, USA).

2.3 | Cell culture

Hepa1-6 cells were maintained in DMEM (Wako Pure Chemical Industries) supplemented with 10% FBS (Nichirei Bioscience Inc., Tokyo, Japan), 200 U/mL penicillin, 100 μg/mL streptomycin, and 10 mM HEPES (Sigma-Aldrich Japan) at 37°C in a humidified atmosphere containing 5% CO_2. CT26 cells were maintained in RPMI-1640 medium (Wako Pure Chemical Industries, Osaka, Japan) supplemented with 10% FBS, 200 U/mL penicillin, 100 μg/mL streptomycin, 10 mM HEPES, and 0.05 mmol/L 2-mercaptoethanol (Sigma-Aldrich) at 37°C in a humidified atmosphere containing 5% CO_2. EG7-OVA cells were maintained in RPMI-1640 medium (Wako Pure Industries, Ltd.) supplemented with 10% FBS, 200 U/mL penicillin, 100 μg/mL streptomycin, 10 mM HEPES, 0.05 mmol/L 2-mercaptoethanol (Sigma-Aldrich) and 100 μg/mL G418 (Wako Pure Industries, Ltd.) at 37°C in a humidified atmosphere containing 5% CO_2. All cell lines were tested to rule out the presence of mycoplasma contamination.

2.4 | Tumor-bearing mouse model

mCherry-transfected Hepa1-6 murine liver cancer cells (1×10^6) were inoculated intrasplenically into C57BL/6 wild-type, *Stat1*$^{-/-}$, or *Tacr2*$^{-/-}$ mice, as described previously.[20] mCherry-positive cells were then visualized using an in vivo imaging system (IVIS Spectrum, Xenogen) and Living Image® Software (Caliper Life Sciences) 14 days after inoculation (day 14). In some experiments, GFP-transfected CT26 murine colon cancer cells (2×10^5) were inoculated intrasplenically into wild-type or *Tacr2*$^{-/-}$ BALB/c mice, as described previously.[21]

Liver tissues from mice were serially sectioned and stained with H&E. The tumorigenesis or metastatic surface was calculated as the total surface occupied by tumorigenesis or metastasis divided by the total area of the liver using ImageJ software. Tumorigenesis images of Hepa1-6-mCherry$^+$ tumors or metastatic colonization images of CT26-GFP$^+$ tumors in livers were evaluated using epi-fluorescence on an IVIS Spectrum ex vivo imaging system (Xenogen) on day 14. Livers and spleens were removed immediately after the mice were euthanized, and collected livers were submerged in PBS on ice. mCherry-labeled Hepa1-6 cells were fluorescently imaged (640/570 em/ex filters). GFP-labeled CT26 cells were fluorescently imaged (540/465 em/ex filters). The conditions were as follows: exposure time = 10 s, lamp level = high, binning = small, and F/Stop = 2. The signal intensity of the tumor burden was expressed as total radiant efficiency (p/s/cm^2/sr)/(μW/cm^2). Images were analyzed using Living Image 4.0 software. The anti-CD8 mAb, anti-NK1.1, or control IgG (200 μg/mouse) was injected intraperitoneally into wild-type C57BL/6 mice on day −1, day 4, and day 9. Poly I:C (10 μg/mouse) or control PBS was injected intraperitoneally into wild-type, *Stat1*$^{-/-}$, or *Tacr2*$^{-/-}$ C57BL/6 mice on day 5 and then every 3 days thereafter. EG7-OVA T lymphoblasts (1×10^6) were inoculated intradermally into wild-type or *Tacr2*$^{-/-}$ C57BL/6 mice. At 14 days after the inoculation, tumor volumes were calculated using the following formula: volume (mm^3) = $\pi/6\times$ length [mm] × width [mm] × height [mm]. Tumor tissues collected from the mice were digested with collagenase (1 mg/mL, Sigma) as previously described.[20,21] Tumor-infiltrating OVA-antigen-specific CD8$^+$ T cells in CD45$^+$7AAD$^-$ cells were evaluated using flow cytometry with T-Select H-2K^b OVA Tetramer-SIINFEKL-PE (Medical & Biological Laboratories Co., Ltd.).

2.5 | Immunohistochemistry

Tumor tissues obtained from Hepa1-6 tumor-bearing wild-type, *Stat1*$^{-/-}$, or *Tacr2*$^{-/-}$ C57BL/6 mice on day 14 were fixed in 4% paraformaldehyde-containing PBS and then embedded in paraffin. After deparaffinization, antigen retrievals for CD4 and CD8 were performed with a reagent kit (pH 9.0) (415211; Nichirei Bioscience, Tokyo, Japan) at 95°C for 10 min and a proteinase K solution (S3004; Dako, Hamburg, Germany) at room temperature for 5 min. Endogenous peroxidase activity was blocked by incubation with 3% hydrogen peroxide at room temperature for 10 min. After washing with TBS, sections were treated with CD4 (D7D2Z) (#25229) and CD8α (D4W2Z) (#98941) mAbs overnight at 4°C. Sections for CD4 and CD8α were incubated with Histofine Simple Stain alone, MAX PO (R) (424144; Nichirei Bioscience) at room temperature for 30 min or rabbit anti-hamster IgG (6215-01; Southern Biotechnology Associates) at room temperature for 30 min, Histofine Simple Stain, MAX PO (R) (424144; Nichirei Bioscience) at room temperature for 30 min, TSA PLUS Biotin KIT (NEL749A001; PerkinElmer, Waltham, MA, USA) at room temperature for 5 min, and VECTASTAIN Elite ABC Reagent (PK6100; Vector Laboratories) at room temperature for 30 min. Protein expression was visualized using 3–3′-diaminobenzidine-4HCL at room temperature for 5 min. All sections were counterstained with Mayer's hematoxylin. The signal strength in tumor tissues was calculated using ImageJ software.

2.6 | Flow cytometry

Hepa1-6 murine liver cancer cells (1×10^6) were intrasplenically injected into wild-type, *Stat1*$^{-/-}$, or *Tacr2*$^{-/-}$ C57BL/6 mice. Tumor tissues, spleen, and periportal lymph nodes were obtained from livers on day 14. The retrieved tissues were minced using scissors and treated with collagenase solution (1 mg/mL, Sigma) as previously described.[20,21] Cell suspensions were treated with anti-CD16/CD32 mAb to Fc receptors for 15 min and stained with 7AAD and fluorescent dye-conjugated anti-CD45, CD4, CD8α, NK1.1, or CD11c mAbs. The signals were detected using a FACSCanto™ II flow cytometry system (BD Biosciences). The surface expression level of CD4 or CD8 in 7AAD-negative CD45-expressing cells was analyzed using FlowJo™ software (Tree Star Inc., Ashland, OR, USA). In some experiments, the percentage of CD4$^+$ T, CD8$^+$ T, NK1.1$^+$ NK, or CD11c$^+$ cells in 7AAD-negative CD45-expressing cells and intracellular granzyme B expression levels of CD4$^+$ T or CD8$^+$ T cells were evaluated by flow cytometry as previously described.[20,21] The change in MFI (ΔMFI) (specific marker MFI − isotype control MFI) was calculated.

2.7 | Intracellular staining

For the detection of cytoplasmic granzyme B, pERK, and IκB expression, spleen cells, or CD8$^+$ T cells sorted from the spleen of normal wild-type, *Stat1*$^{-/-}$, or *Tacr2*$^{-/-}$ C57BL/6 mice were fixed in BD Cytofix/Cytoperm (BD Bioscience) solution after cell surface staining with 7-AAD alone or combined with anti-CD45 mAb and anti-CD8 mAb. Intracellular staining was performed in BD Perm/Wash buffer containing anti-granzyme B mAb or PerFix EXPOSE buffer 3 (Beckman Coulter) containing anti-pERK mAb or anti-IκB mAb. Expression levels were evaluated using a FACSCanto™ II system (BD Bioscience) and analyzed using FlowJo™ software (Tree Star). Corresponding isotype controls were also used.

2.8 | ELISA

Spleen cells or CD8$^+$ T cells sorted from the spleen tissues of normal wild-type, *Stat1*$^{-/-}$, or *Tacr2*$^{-/-}$ C57BL/6 mice were stimulated with or without anti-CD3 and anti-CD28 mAbs (50 ng/mL) for 24 h. IFN-γ or interleukin (IL)-2 levels in the supernatant were determined using OptEIA™ Mouse IFN-γ or OptEIA™ Mouse IL-2 ELISA kits (BD Biosciences) in accordance with the manufacturer's instructions.

2.9 | Western blotting

CD8$^+$ T cells (1×10^7) obtained from the spleen tissues of wild-type or *Tacr2*$^{-/-}$ C57BL/6 mice were stimulated with anti-CD3 and anti-CD28 mAbs (50 ng/mL) for 20 min, and total and phosphorylated ERK, IκB, and α-tubulin levels in cell lysates were detected by western blotting. Cells were lysed using RIPA buffer (Thermo) (Tris HCl 25 mM [pH 7.6], NaCl 150 mM, 1% sodium deoxycholate, 1% Nonidet P-40, 0.1% SDS, protease inhibitor cocktail [Sigma-Aldrich], and phosphatase inhibitor cocktail [Nacalai Tesque]). Proteins were then diluted in RIPA buffer and 3× Laemmli Sample Buffer (Bio-Rad, Hercules, CA, USA), incubated at 95°C for 5 min, resolved by e-PAGEL (E-T1020L) gel electrophoresis (ATTO), transferred to a polyvinylidene difluoride membrane, and blocked in Blocking ONE-P (Nacalai Tesque) for 1 h at room temperature. Membranes were then incubated with antibodies (phospho-ERK 1:1000, IκBα 1:1000, α-tubulin 1:1000) at 4°C overnight, followed by HRP-conjugated anti-rabbit IgG (1:5000) or HRP-conjugated anti-mouse IgG (1:5000) secondary antibody at room temperature for 1 h. The protein bands were visualized using an ImageQuant™ LAS 4000 mini system (Bio-Sciences) and ImageQuant™ LAS 4000 software (Bio-Sciences) and analyzed and quantified using ImageJ software. The membranes were reprobed after removing bound antibodies using Western Blot Stripping Buffer (TaKaRa).

2.10 | PCR analysis

CD8$^+$ T cells isolated from the spleen of wild-type and *Stat1*$^{-/-}$ or *Tacr2*$^{-/-}$ C57BL/6 mice were treated with anti-CD3 mAb (50 ng/mL) and anti-CD28 mAb (50 ng/mL) for 12 h. Total RNA was extracted from spleen cells or CD8$^+$ T cells after stimulation using ISOGEN (Nippon Gene, Tokyo, Japan; #311-07361) in accordance with the manufacturer's instructions. RNA concentration was measured using a NanoDrop spectrophotometer (Thermo Fisher Scientific, #ND-1000). First-strand cDNA was synthesized using 1 mg of total RNA with ReverTra Ace® qPCR RT Master Mix (Toyobo, Osaka, Japan) and then amplified on a thermal cycler (GeneAmp PCR System 9700, Applied Biosystems, Waltham, Massachusetts, USA). Template DNA was used for a final PCR reaction volume of 10 μL. The murine gene expression levels of NK1R (*Tacr1*), NK2R (*Tacr2*), tachykinin precursor 1 (*Tac1*), STAT1 (*Stat1*), IFN-γ, granzyme B, and β-actin (*Actb*) were amplified and detected using FastStart SYBR Green Master (Roche) and StepOnePlus™ (Applied Biosystems). The primer sequences used in this study were as follows: *Tac1* (left: 5′-ggcactggaaatgatctgg-3′, right: 5′-aatctttctcaaattctcaccttca-3′); *Tacr1* (left: 5′-ggatggacaaggtttgcag-3′, right: 5′-tgacaaaaactagaagcggatg-3′); *Tacr2* (left: 5′-gcaggtc tacctggcactct-3′, right: 5′-ggaatccagagcgaaacct-3′); *Stat1* (left: 5′-tgagatgtcccggatagtgg-3′, right: 5′-cgccagagagaaattcgtgt-3′); *Ifna* (left: 5′-tcaagccatccttgtgctaa-3′, right: 5′-gtcttttgatgtgaaga ggttcaa-3′); *Ifnb* (left: 5′-ctggcttccatcatgaacaa-3′, right: 5′-agag ggctgtggtggagaa-3′) *Ifng* (left: 5′-atctggaggaactggcaaaa-3′, right: 5′-ttcaagacttcaaagagtctgagg-3′); *gzmb* (left: 5′-tgctgctcactgt-gaaggaa-3′, right: 5′-ttaccatagggataacttgctg-3′) and *Actb* (left: 5′-aaggccaaccgtgaaaagat-3′, right: 5′-gtggtacgaccagaggcatac-3′). Sample signals were normalized to the reference gene *Actb* using the $^{\Delta\Delta}$Ct method: $^{\Delta}Ct = {}^{\Delta}Ct_{sample} - {}^{\Delta}Ct_{reference}$. Percentages relative to the control sample were then calculated for each sample.

2.11 | Statistical analysis

In vitro experiments were repeated two to four times. In vivo experiments (4–10 mice/group) were performed two to three times independently. Means and SDs were calculated for each dataset. Significant differences were determined using two-tailed Student's *t*-tests or Tukey's honestly significant difference (HSD) test. A *p*-value <0.05 was considered significant. Data were analyzed using Microsoft (R) Excel for Mac (version 16.61.1) or JMP statistical software for Windows (version 16.1.0; SAS Institute Inc).

3 | RESULTS

3.1 | Poly I:C administration induces type I and type II IFNs and CD8$^+$ T cells are involved in the suppression of the tumorigenesis of liver cancer cells in vivo

First, we established a liver cancer model by intrasplenic injection with Hepa1-6 murine liver cancer cells into wild-type C57BL/6 mice. Five days after inoculation, Hepa1-6-bearing mice were administered poly I:C, a Toll-like receptor 3 (TLR3) ligand, every 3 days (Figure 1A). Poly I:C treatment significantly enhanced *Ifna*, *Ifnb*, and *Ifng* gene expression levels in spleen cells (Figure 1B) and reduced the tumorigenesis of liver cancer cells in the liver (Figure 1C,D). We found that CD4$^+$ T cell and CD8$^+$ T cell infiltration in the tumor mass, but not the total liver, was significantly increased by the administration of poly I:C (Figure 1E,F). The poly I:C treatment significantly induced granzyme B-expressing CD8$^+$ T cells in both liver and spleen of Hepa1-6-bearing liver cancer model, although those for CD4$^+$ T cells were not altered (Figure S1). Furthermore, we confirmed that the depletion of CD8$^+$ T cells or NK1.1$^+$ NK cells from liver cancer model mice significantly abolished the antitumor effect of poly I:C treatment (Figure 1G,H and S2). These data suggested that poly I:C treatment induces antitumor CD8$^+$ T cells as well as NK1.1$^+$ NK cells to eliminate liver cancer cells in vivo.

3.2 | STAT1 is crucial for the induction and activation of antitumor effector T cells in vivo

Next, we investigated the effect of STAT1, a transcriptional activator and downstream factor of IFN signaling, on the induction of antitumor immunity and tumorigenesis of liver cancer cells in vivo. The tumorigenesis of liver cancer cells was significantly augmented in STAT1-deficient (*Stat1*$^{-/-}$) mice compared with that in wild-type (*Stat1*$^{+/+}$) mice (Figure 2A,B). Then, we examined the accumulation of CD4$^+$ T cells and CD8$^+$ T cells in liver cancer-bearing mice. We found that the frequency of tumor-infiltrating CD4$^+$ T cells and CD8$^+$ T cells was significantly reduced in the liver of *Stat1*$^{-/-}$ mice compared with that in *Stat1*$^{+/+}$ mice (Figure 2C,D). Moreover, we confirmed that poly I:C treatment did not have antitumor effects in the liver of *Stat1*$^{-/-}$ mice (Figure 2E,F). These data suggest that the activation of STAT1-mediated signaling is required for the induction of antitumor effector T cells in the tumor microenvironment.

3.3 | IFN-γ induces NK2R expression in a STAT1-dependent manner, and NK2R-mediated NKA signaling augments the immune responses of CD8$^+$ T cells in vitro

To elucidate the mechanism underlying the induction of antitumor effector cells through the IFN–STAT1 axis, we performed the following in vitro experiments. We found that IFN-γ but not IL-2 production by STAT1-deficient spleen cells was reduced compared with the levels in wild-type cells after anti-CD3 mAb and anti-CD28 mAb stimulation (Figure 3A). In this experiment, we confirmed

FIGURE 1 Poly I:C administration promotes the infiltration of antitumor CD8$^+$ cells into tumor microenvironments and suppresses the tumorigenesis of liver cancer cells in vivo. mCherry-transfected Hepa1-6 murine liver cancer cells (1×10^6) were intrasplenically injected into wild-type C57BL/6 mice (day 0). Poly I:C (10 μg/mouse) or control PBS was injected intraperitoneally into wild-type C57BL/6 mice on day 5 and then every 3 days thereafter. (A) Experimental scheme is shown. (B) Relative gene expression levels of *Ifna*, *Ifnb*, and *Ifng* relative to *Actb* in spleen cells from Hepa1-6 tumor-bearing wild-type C57BL/6 mice on day 14 were evaluated, and means and SDs are indicated ($n = 6$–8 mice/group, more than two independent experiments). *$p<0.05$ by Student's *t*-test. (C) Tumorigenesis of Hepa1-6 cells in the liver was evaluated using an imaging system on day 14. Representative images are shown. Photon flux ratios were evaluated from the images ($n = 6$–8 mice/group, more than three independent experiments). Means and SDs are shown. *$p<0.05$ by Student's *t*-test. (D) H&E staining of liver tissue was performed 14 days after inoculation. Representative micrographs are shown ($n = 4$ mice/group). Bars, 500 μm. Ratios of tumor area relative to total liver tissue area were calculated by ImageJ software. Means and SDs are shown. *$p<0.05$ by Student's *t*-test. (E) Immunohistochemistry was performed to evaluate CD4$^+$ and CD8$^+$ cells in the tumor microenvironment on day 14. Representative micrographs are shown (the zoomed areas are ×6 magnification; $n = 4$ mice/group). Bars, 100 μm. Integrated density of cell signal strength was calculated by ImageJ software. Means and SDs are shown. *$p<0.05$ by Student's *t*-test. (F) CD4$^+$ and CD8$^+$ cells obtained from the livers on day 14 were evaluated by flow cytometry. Representative images are shown. Percentages of CD4$^+$ and CD8$^+$ cells among total 7AAD$^-$CD45$^+$ cells were calculated ($n = 4$ mice/group, two independent experiments), and means and SDs are shown. * $p<0.05$ by Student's *t*-test. (G, H) Anti-CD8 antibodies or control IgG were injected into wild-type and poly I:C-treated Hepa1-6-bearing mice on days −1, 4, and 9. Tumorigenesis of Hepa1-6 cells in the liver was evaluated using an imaging system and H&E staining on day 14 ($n = 8$–10 mice/group, two independent experiments). Representative images and means with SDs for photon flux or tumor area percentages are shown. *$p<0.05$ by Student's *t*-test.

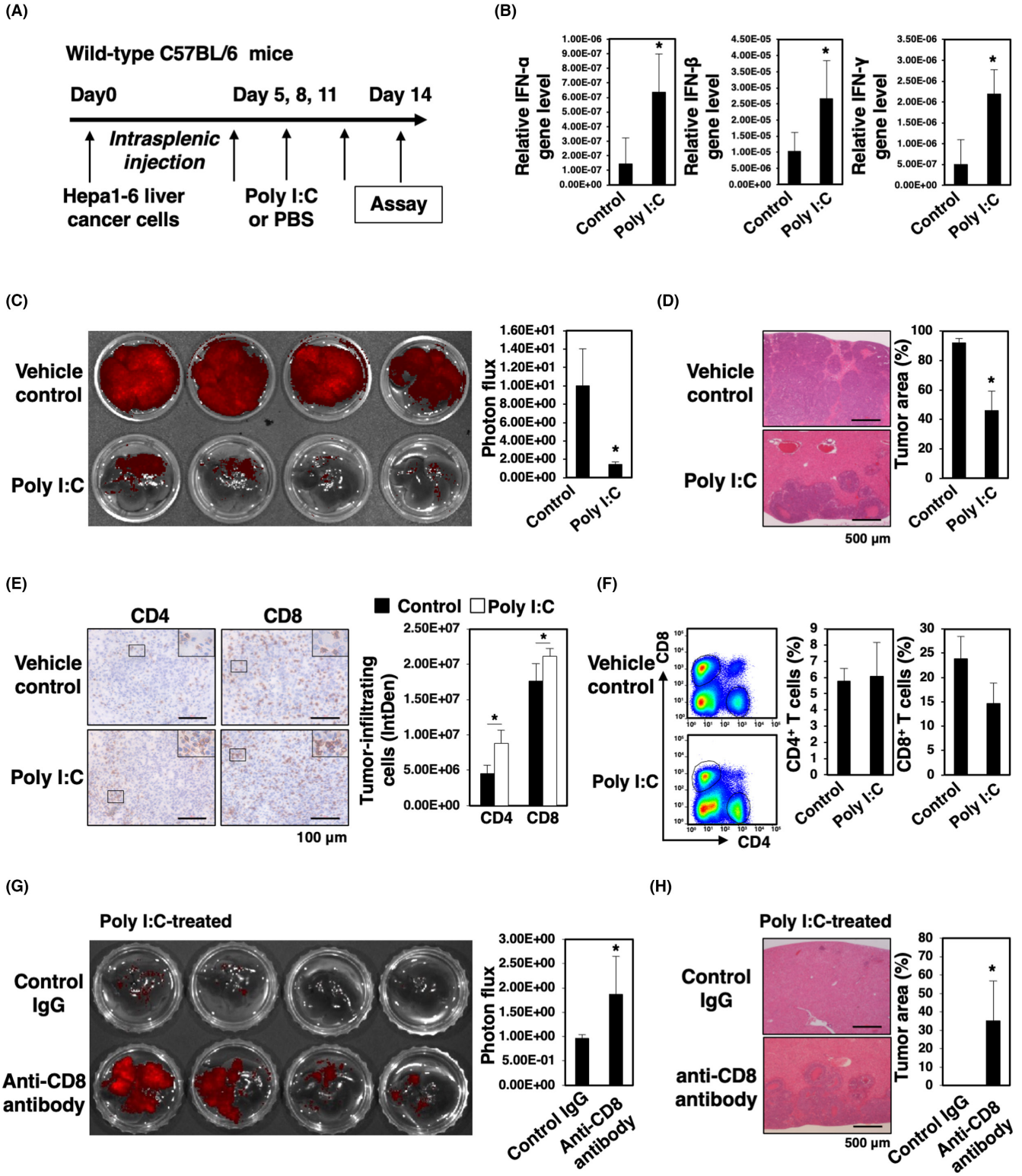

that the induction of IFN-γ^{+}CD8^{+} T cells was significantly reduced in STAT1-deficient spleen cells compared with wild-type cells after CD3 and CD28 stimulation, although the frequency of the CD62L^{low}CD44^{hi}CD8^{+} T cells was augmented and CD62L^{hi}CD44^{hi} CD8^{+} T cells were decreased in the STAT1-deficient spleen cells compared with the wild-type cells (Figure S3). Furthermore, STAT1 deficiency significantly reduced granzyme B production by anti-CD3 mAb- and anti-CD28 mAb-stimulated CD8^{+} T cells in spleen cells (Figure 3B). To identify the target molecules of STAT1, CD8^{+} T cells were isolated from *Stat1*$^{+/+}$ and *Stat1*$^{-/-}$ mice and stimulated with IFN-γ. In this study, we revealed that NK2R (*Tacr2*), preprotachykinin (*Tac1*) encoding substance P and NKA neuropeptides,

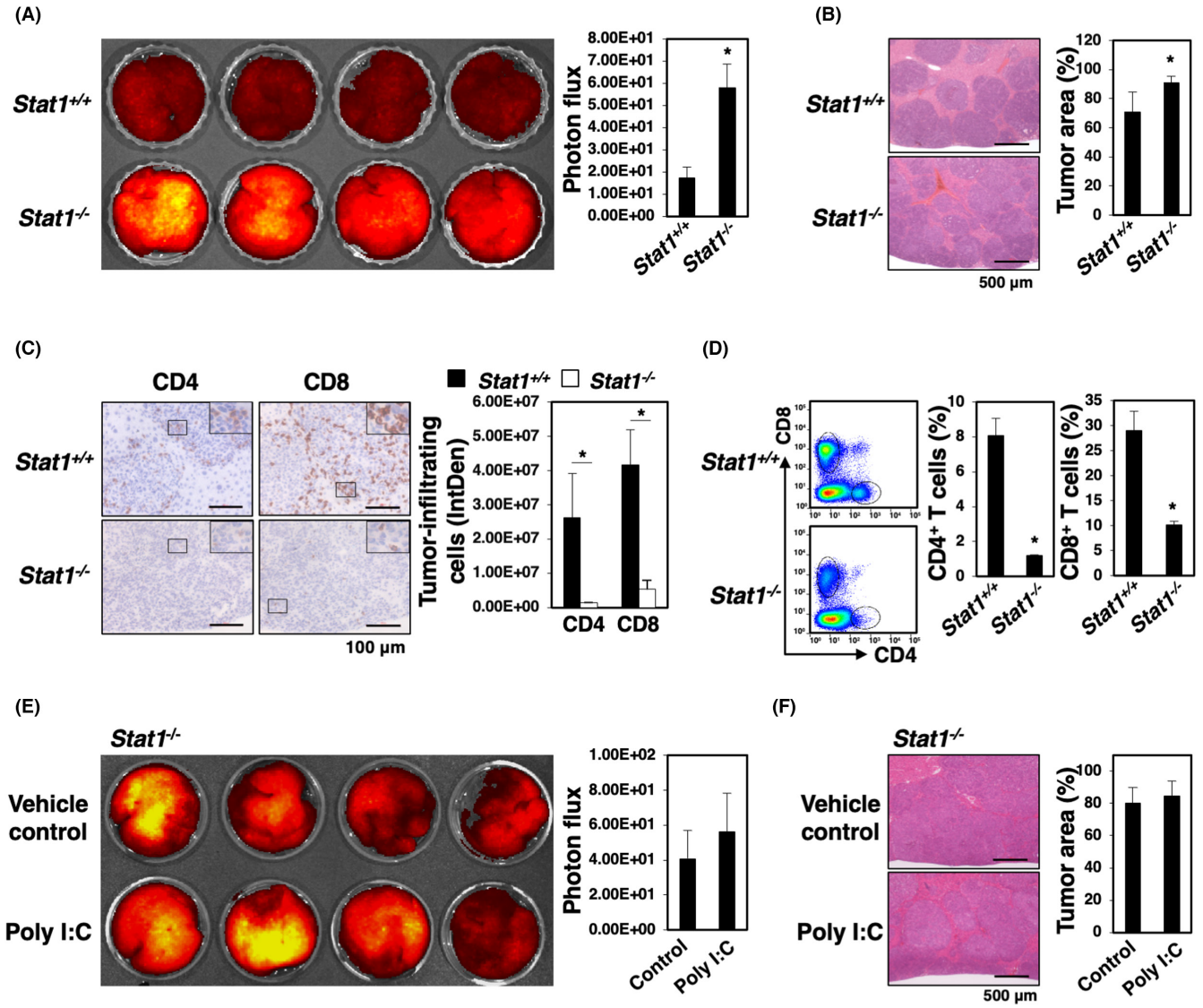

FIGURE 2 STAT1 is crucial for the induction of antitumor effector cells in vivo. mCherry-transfected Hepa1-6 murine liver cancer cells (1×10^6) were intrasplenically injected into wild-type (*Stat1*$^{+/+}$) and STAT1-deficient (*Stat1*$^{-/-}$) C57BL/6 mice (day 0). (A) Tumorigenesis of mCherry-expressing Hepa1-6 cells in the liver was evaluated using an imaging system on day 14. Representative images are shown. Photon flux was evaluated from the images ($n = 6$–9 mice/group, more than three independent experiments). Means and SDs are shown. *$p < 0.05$ by Student's *t*-test. (B) H&E staining of liver tissues was performed 14 days after inoculation. Representative micrographs are shown ($n = 4$ mice/group). Bars, 500 μm. Ratios of tumor area relative to total liver tissue area were calculated by ImageJ software. Means and SDs are shown. *$p < 0.05$ by Student's *t*-test. (C) Immunohistochemistry was performed to evaluate CD4$^+$ and CD8$^+$ cells in the tumor microenvironment on day 14. Representative micrographs are shown (the zoomed areas are ×6 magnification; $n = 2$ mice/group). Bars, 100 μm. Integrated density of cell signal strength was calculated by ImageJ software. Means and SDs are shown. *$p < 0.05$ by Student's *t*-test. (D) CD4$^+$ and CD8$^+$ cells obtained from the livers on day 14 were evaluated by flow cytometry. Representative images are shown. Percentages of CD4$^+$ and CD8$^+$ cells among total 7AAD$^-$CD45$^+$ cells were calculated. Means and SDs are shown ($n = 4$ mice/group, two independent experiments). *$p < 0.05$ by Student's *t*-test. (E, F) Poly I:C or the vehicle control was injected into Hepa1-6-bearing *Stat1*$^{-/-}$ mice on days 5, 8, and 11. Tumorigenesis of Hepa1-6 cells in the liver was evaluated using an imaging system and H&E staining on day 14 ($n = 7$ or 8 mice/group, three independent experiments). Representative images and means with SDs for photon flux or tumor area percentages are shown. *$p < 0.05$ by Student's *t*-test.

and STAT1 (*Stat1*) gene expression levels were enhanced in CD8$^+$ T cells in a STAT1-dependent manner (Figure 3C). Although a decreasing trend in NK1R (*Tacr1*) was observed, it did not reach statistical significance. These results suggest that NK2R expression might be related to the antitumor effector function of CD8$^+$ T cells.

To address the involvement of NK2R-mediated NKA signaling in the cytokine production and cytotoxicity of CD8$^+$ T cells, CD8$^+$ T cells were stimulated with an NKA ligand together with anti-CD3 antibodies in vitro. IFN-γ and granzyme B but not IL-2 production by anti-CD3 mAb-stimulated CD8$^+$ T cells were significantly

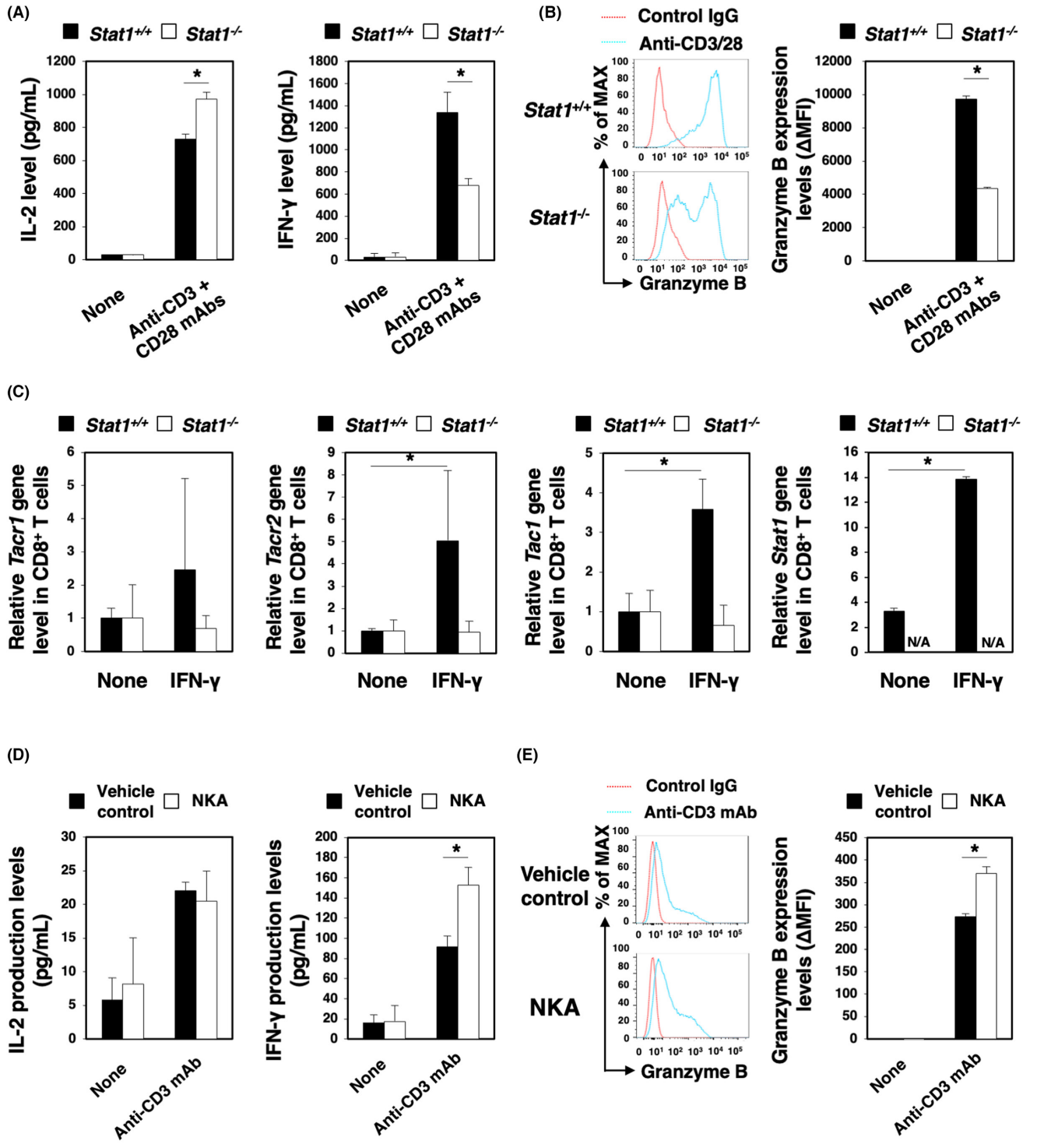

FIGURE 3 Neurokinin-2 receptor (NK2R) is involved in the activation of type 1 immune responses in a STAT1-dependent manner in vitro. Spleen cells of wild-type (*Stat1*$^{+/+}$) and STAT1-deficient (*Stat1*$^{-/-}$) C57BL/6 mice were treated with anti-CD3 and CD28 mAbs for 24 h. (A) IL-2 and IFN-γ production levels were evaluated by ELISAs. Mean and SDs ($n = 4$/group) are shown. *$p < 0.05$ by Tukey's HSD test. (B) Granzyme B production levels in CD8$^+$ T cells in the spleen were determined by flow cytometry. Representative images are shown. ΔMFIs against each isotype control were calculated, and the means and SDs are shown ($n = 4$/group, cumulative results from three independent experiments). *$p < 0.05$ by Tukey's HSD test. (C) CD8$^+$ T cells isolated from the spleen of wild-type (*Stat1*$^{+/+}$) and STAT1-deficient (*Stat1*$^{-/-}$) C57BL/6 mice were stimulated with IFN-γ for 12 h. Gene expression levels of NK1R (*Tacr1*), NK2R (*Tacr2*), tachykinin precursor 1 (*Tac1*), and STAT1 (*Stat1*) were determined by quantitative PCR. Means and SDs are shown ($n = 4$ mice/group, two independent experiments). *$p < 0.05$ by Student's *t*-test. (D, E) CD8$^+$ T cells isolated from the spleen of wild-type C57BL/6 mice were stimulated with anti-CD3 mAb in the presence of an NK2R selective agonist (NKA, 1 μM) or vehicle control for 24 h. IL-2 and IFN-γ production levels were evaluated by ELISAs. Mean and SDs ($n = 4$/group) are shown. *$p < 0.05$ by Tukey's HSD test. Granzyme B production levels in CD8$^+$ T cells were determined by flow cytometry. Representative images are shown. ΔMFIs against each isotype control were calculated, and the means and SDs are shown ($n = 4$/group, cumulative results from two independent experiments). *$p < 0.05$ by Tukey's HSD test.

augmented by the addition of the NKA ligand in vitro (Figure 3D,E). The gene expression levels of IFN-γ and granzyme B in CD8$^+$ T cells were significantly enhanced by anti-CD3 mAb stimulation combined with the NKA ligand (Figure S4). These findings suggest that NK2R-mediated NKA signaling might be involved in antitumor immune responses through NK2R expression in CD8$^+$ T cells.

3.4 | STAT1-mediated NK2R expression is involved in the induction of effector CD8$^+$ T cells through the activation of ERK1/2 and NF-κB signaling pathways

We further investigated the effect of NK2R expression in CD8$^+$ T cells on their function as antitumor effector cells in vitro. CD8$^+$ T

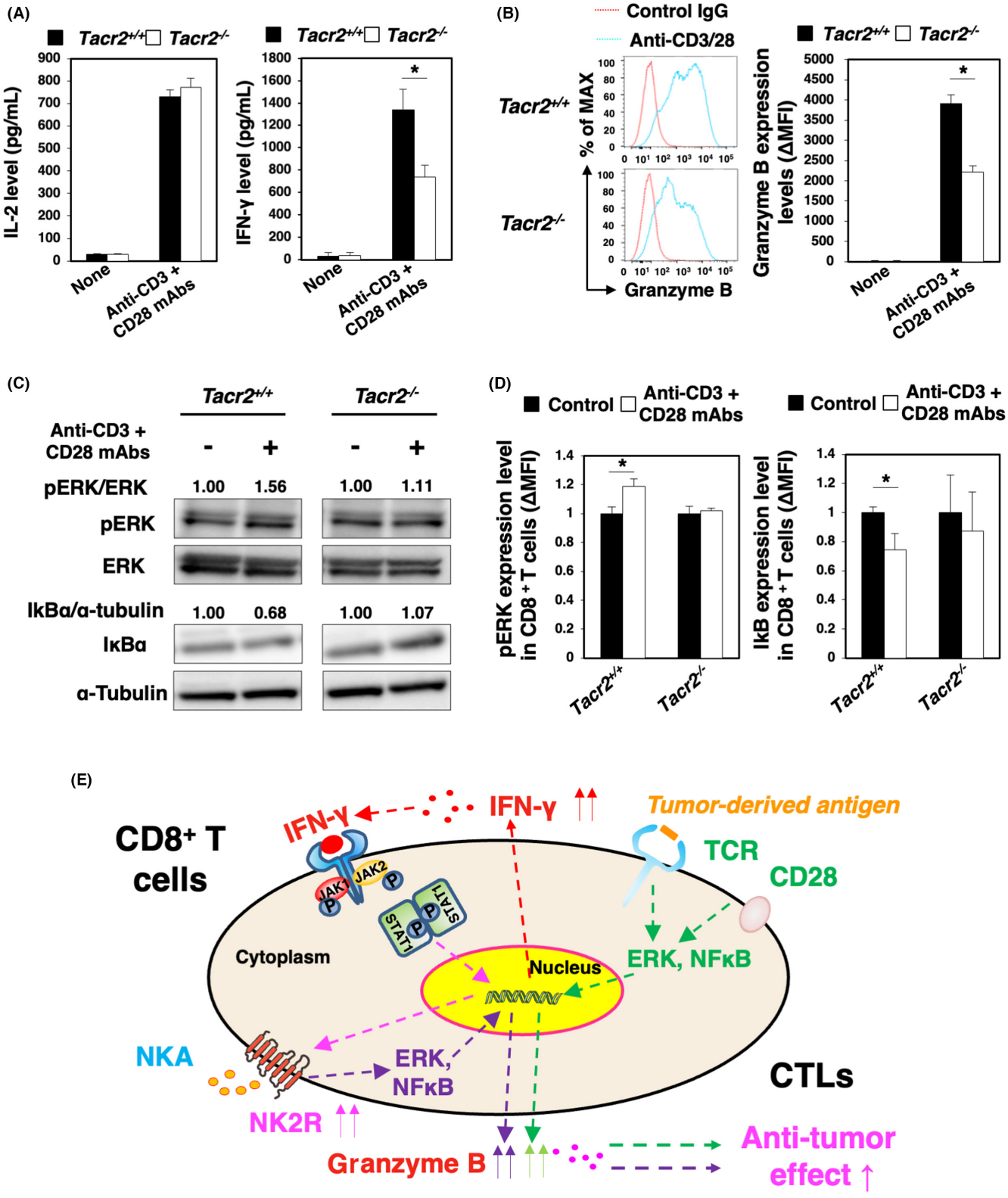

FIGURE 4 STAT1-mediated NK2R expression is involved in the induction of antitumor killer T cells through the activation of ERK and NF-κB signaling pathways. $CD8^+$ T cells isolated from the spleen of wild-type (*Tacr2*$^{+/+}$) and NK2R-deficient (*Tacr2*$^{-/-}$) C57BL/6 mice were treated with anti-CD3 and CD28 mAbs for 24 h. (A) IL-2 and IFN-γ production levels were evaluated by ELISAs. Mean and SDs ($n = 4$/group) are shown. $^*p < 0.05$ by Tukey's HSD test. (B) Granzyme B production levels in $CD8^+$ T cells in the spleen were determined by flow cytometry. Representative images are shown. ΔMFIs against each isotype control were calculated, and the means and SDs are shown ($n = 4$/group, cumulative results from two independent experiments). $^*p < 0.05$ by Tukey's HSD test. (C) $CD8^+$ T cells isolated from the spleen of *Tacr2*$^{+/+}$ and *Tacr2*$^{-/-}$ mice were stimulated with anti-CD3 and CD28 mAbs for 20 min. Expression levels of phosphorylated ERK (pERK1/2) and total ERK1/2 or total IκB and α-Tubulin were determined by western blotting. Representative images and the relative expression levels of pERK1/2 and IκB are shown. (D) $CD8^+$ T cells isolated from the spleen of *Tacr2*$^{+/+}$ and *Tacr2*$^{-/-}$ mice were stimulated with anti-CD3 and CD28 mAbs for 20 min. Expression levels of p-ERK1/2 and IκB were evaluated by flow cytometry. ΔMFIs against each isotype control were calculated, and means and SDs shown ($n = 4$ mice/group, two independent experiments). $^*p < 0.05$ by Student *t*-test. (E) Proposed model of the present study.

cells from *Tacr2*$^{+/+}$ and *Tacr2*$^{-/-}$ mice were stimulated with anti-CD3 and anti-CD28 antibodies. The production of IFN-γ but not IL-2 from NK2R-deficient $CD8^+$ T cells was significantly lower than that in wild-type $CD8^+$ T cells (Figure 4A). In this experiment, we confirmed that the frequency of $CD62L^{low}CD44^{hi}CD8^+$ T cells and induction of IFN-γ^+ $CD8^+$ T cells were significantly reduced and $CD62L^{hi}CD44^{hi}CD8^+$ T cells were significantly increased in NK2R-deficient spleen cells compared with wild-type cells after the CD3 and CD28 stimulation (Figure S5). Furthermore, granzyme B production by anti-CD3 mAb- and anti-CD28 mAb-stimulated NK2R-deficient $CD8^+$ T cells was significantly reduced compared with that in wild-type $CD8^+$ T cells (Figure 4B). The gene expression levels of IFN-γ and granzyme B in anti-CD3 mAb-stimulated $CD8^+$ T cells were significantly reduced under NK2R deficiency (Figure S6). These data suggest that STAT1-dependent NK2R expression might be related to the induction and maintenance of antitumor killer T cells.

Then, we investigated the involvement of NK2R in the TCR-mediated signaling pathways that activate $CD8^+$ T cells. The phosphorylation level of ERK1/2 was augmented in $CD8^+$ T cells isolated from *Tacr2*$^{+/+}$ but not *Tacr2*$^{-/-}$ mice after stimulation with anti-CD3 and anti-CD28 antibodies (Figure 4C,D). Furthermore, the protein level of IκB was unchanged in *Tacr2*$^{-/-}$ $CD8^+$ T cells after stimulation with anti-CD3 and anti-CD28 antibodies but reduced in *Tacr2*$^{+/+}$ $CD8^+$ T cells (Figure 4C,D). These findings suggest that stimulation via TCRs and costimulatory molecules on $CD8^+$ T cells induces IFN-γ production, and IFN-γ-dependent STAT1 activation enhances NK2R expression levels. Subsequently, NK2R-mediated NKA signaling further augments IFN-γ and granzyme B production by effector T cells through the activation of the ERK1/2 and NF-κB signaling pathways (Figure 4E).

3.5 | NK2R is involved in the induction of antitumor immunity to eliminate liver cancer cells in vivo

We then investigated the effect of NK2R on the tumorigenesis of liver cancer cells in liver tissues. To this end, we intrasplenically inoculated Hepa1-6 murine liver cancer cells into wild-type (*Tacr2*$^{+/+}$) C57BL/6 mice and NK2R-deficient (*Tacr2*$^{-/-}$) mice. We noted that the tumorigenesis of Hepa1-6 cells was significantly augmented in *Tacr2*$^{-/-}$ mice compared with that in *Tacr2*$^{+/+}$ mice (Figure 5A,B). Moreover, we found that tumor-infiltrating $CD4^+$ T and $CD8^+$ T cells were significantly reduced in *Tacr2*$^{-/-}$ mice (Figure 5C). The infiltration degrees of $CD4^+$ T, $CD8^+$ T, $NK1.1^+$, and $CD11c^+$ cells into Hepa1-6-bearing liver tissues and the frequency of $CD4^+$ T cells in the spleen were significantly reduced in *Tacr2*$^{-/-}$ mice compared with those in *Tacr2*$^{+/+}$ mice (Figures 5D and S7A), although the frequency of $CD8^+$ T, $NK1.1^+$, and $CD11c^+$ cells in the spleen and $CD4^+$ T, $CD8^+$ T, $NK1.1^+$, and $CD11c^+$ cells in the periportal lymph nodes was not altered (Figure S7B,C). We found that tumor growth of OVA-expressing EG7 cells was enhanced in the NK2R-deficient mice compared with the wild-type mice (Figure S8A) and further revealed that the induction of OVA-antigen-specific $CD8^+$ T cells was significantly reduced in the NK2R-deficient mice inoculated with OVA-expressing EG7 cells compared with the wild-type mice (Figure S8B). In this study, we confirmed that the metastatic colonization of colon cancer cells in the liver was significantly augmented by NK2R deficiency (Figure S9A,B). In this metastatic liver cancer model, the infiltration of $CD4^+$ T and $CD8^+$ T cells into the tumor tissues of *Tacr2*$^{-/-}$ mice was reduced compared with that in *Tacr2*$^{+/+}$ mice (Figure S9C). These data suggest that NK2R activation is involved in the induction of antigen-specific antitumor effector T cells to eliminate cancer cells in liver tissues in vivo. Finally, we evaluated the antitumor effect of poly I:C in *Tacr2*$^{+/+}$ and *Tacr2*$^{-/-}$ mice. Poly I:C injection did not significantly alter the reduced tumorigenesis in poly I:C-treated NK2R-deficient mice (Figure 5E,F). These data suggest that IFN-γ, NK2R, and $CD8^+$ T cells are involved in the reduced tumorigenesis of liver cancer cells following poly I:C administration.

4 | DISCUSSION

Tachykinins act through G protein-coupled receptors (GPCRs) in the peripheral and central nervous systems to control various physiological functions.[22–24] NKA, a ligand of NK2R, is known to control several vital responses, such as airway contraction, vasodilatation, and vascular permeability.[25–27] In this study, we found that the *Tac1* gene, coding NKA, was induced in $CD8^+$ T

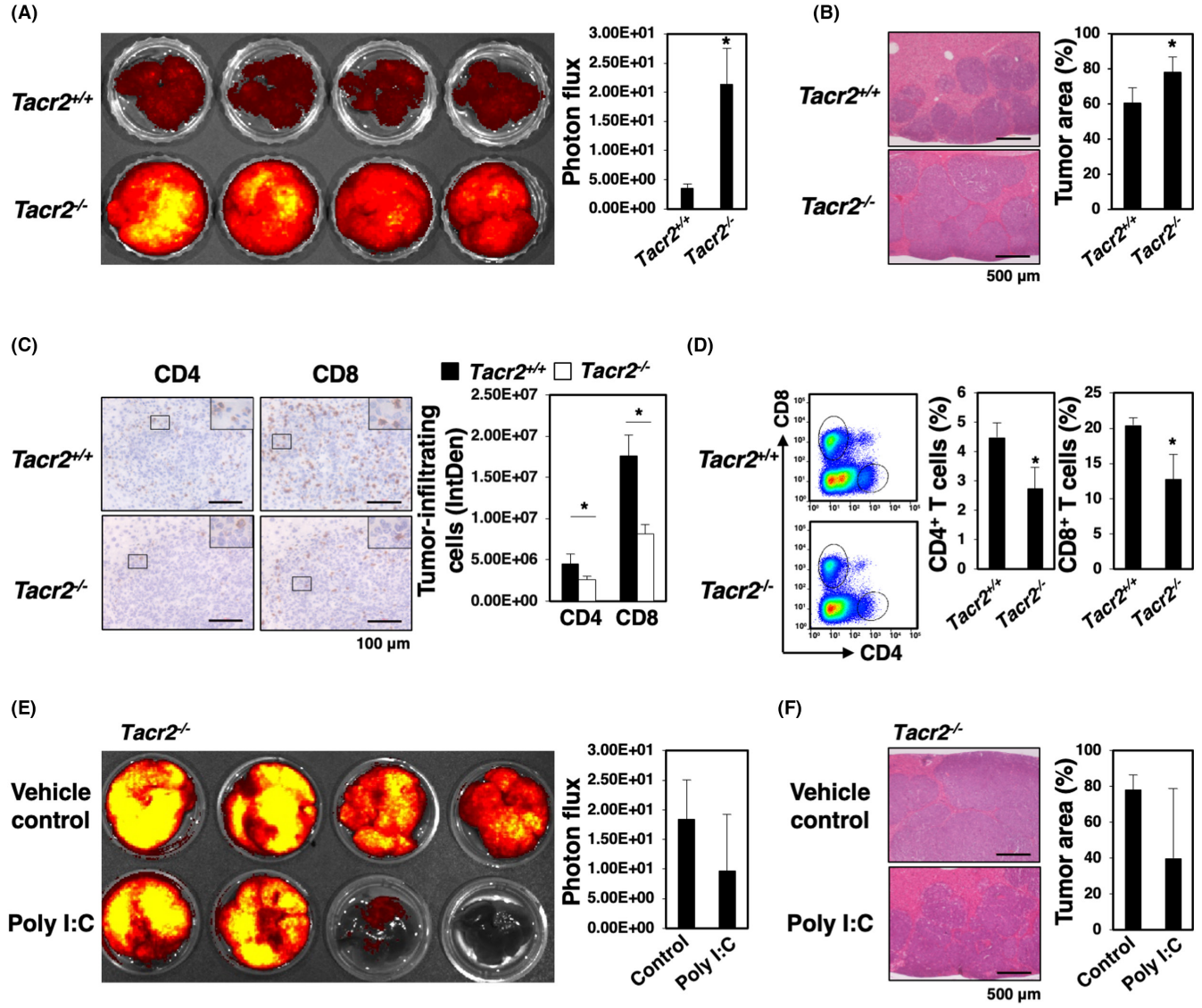

FIGURE 5 NK2R is related to the induction of antitumor effector cells in poly I:C-treated liver cancer-bearing mice in vivo. mCherry-transfected Hepa1-6 murine liver cancer cells (1×10^6) were intrasplenically injected into wild-type (*Tacr2*$^{+/+}$) and NK2R-deficient (*Tacr2*$^{-/-}$) C57BL/6 mice (day 0). (A) Tumorigenesis of mCherry-expressing Hepa1-6 cells in the liver was evaluated using an imaging system on day 14. Representative images are shown. Photon flux was evaluated from the images ($n = 6$–9 mice/group, more than three independent experiments). Means and SDs are shown. $^*p < 0.05$ by Student's *t*-test. (B) H&E staining of liver tissues was performed 14 days after inoculation. Representative micrographs are shown ($n = 4$ mice/group). Bars, 500 μm. Ratios of tumor area relative to total liver tissue area were calculated by ImageJ software. Means and SDs are shown. $^*p < 0.05$ by Student's *t*-test. (C) Immunohistochemistry was performed to evaluate CD4$^+$ and CD8$^+$ cells in the tumor microenvironment on day 14. Representative micrographs are shown (the zoomed areas are 6× magnification; $n = 4$ sections/group). Bars, 100 μm. Integrated density of cell signal strength was calculated by ImageJ software. Means and SDs are shown. $^*p < 0.05$ by Student's *t*-test. (D) CD4$^+$ and CD8$^+$ cells obtained from the livers on day 14 were evaluated by flow cytometry. Representative images are shown. Percentages of CD4$^+$ and CD8$^+$ cells among total 7AAD$^-$CD45$^+$ cells were calculated. Means and SDs are shown ($n = 4$ mice/group, two independent experiments). $^*p < 0.05$ by Student's *t*-test. (E, F) Poly I:C or the vehicle control was injected into Hepa1-6-bearing *Tacr2*$^{-/-}$ mice on days 5, 8, and 11. Tumorigenesis of Hepa1-6 cells in the liver was evaluated using an imaging system and H&E staining on day 14 ($n = 7$ or 8 mice/group, three independent experiments). Representative images and means with SDs for photon flux or tumor area percentages are shown. $^*p < 0.05$ by Student's *t*-test.

cells after IFN-γ stimulation in a STAT1-dependent manner. Our previous study revealed that poly I:C administration into CT26 tumor-bearing mice induced *Tac1* gene expression in dendritic cells and cancer cells in the tumor microenvironment.[10] Based on these findings, we speculated that NKA might be produced by CD8$^+$ T cells, dendritic cells, and cancer cells in addition to cells of the sensory nervous system in the tumor microenvironment. Previous studies indicated that NK2R expression was observed in neurons,[28] macrophages,[29] dendritic cells,[8,9] and cancer cells.[5,10] We reported that NKA and NK2R expression were increased in

dendritic cells in a STAT1-dependent manner, and the enhanced NK2R expression-mediated NKA signaling augmented the induction of antigen-specific $CD4^+$ T cells and $CD8^+$ T cells.[8,9] However, the roles of NK2R expression in antitumor immunity in tumor-bearing hosts are unclear. In this study, we revealed that IFN-γ augmented NK2R expression levels in $CD8^+$ T cells in a STAT1-dependent manner, and NKA stimulation induced IFN-γ and granzyme B production by $CD8^+$ T cells involved in the activation of ERK1/2 and NF-kB cascades. Furthermore, we confirmed that the STAT1–NK2R axis was associated with the infiltration of $CD8^+$ T cells into the tumor tissues of a liver cancer-bearing model. Accordingly, we speculated that NK2R-mediated NKA signaling was involved in antitumor immune responses in vivo.

Here, we revealed that NKA stimulation enhanced the production levels of IFN-γ and granzyme B in $CD8^+$ T cells. NK2R and NK1R belong to the rhodopsin-like family 1 of GPCRs, which plays a crucial role in intracellular signaling.[7,30] GPCR ligand-mediated activation of ERK1/2 and NF-κB is involved in multiple cellular physiological functions.[31–33] A previous study showed that NK1R-mediated signaling enhanced the viability of TCR-activated $CD8^+$ T cells by activating the NF-κB signaling pathway.[34] In this study, we found that the phosphorylation of ERK1/2 was augmented in wild-type but not in NK2R-deficient $CD8^+$ T cells, and the protein level of IκB was unchanged in NK2R-deficient $CD8^+$ T cells but reduced in wild-type $CD8^+$ T cells after TCR stimulation. From these data, we speculate that the IFN–STAT1–NK2R axis is involved in the induction of antitumor effector $CD8^+$ T cells through the activation of ERK1/2 and NF-κB signaling pathways.

The introduction of effector T cells into the tumor microenvironment is crucial for effective cancer immunotherapy. The TLR3 ligand poly I:C induces STAT1 phosphorylation in T cells, dendritic cells, and macrophages[35–37] and is a powerful agent to induce antitumor immunity by increasing the production of type I and type II IFNs in tumor-bearing hosts.[37,38] In this study, we confirmed that the administration of poly I:C promoted the infiltration of antitumor effector T cells in the tumor tissues of a liver cancer model and significantly suppressed tumorigenesis in a STAT1-dependent manner. Furthermore, we found that the infiltration of $CD8^+$ T cells in tumor tissues was significantly reduced, and the tumorigenesis of liver cancer cells was augmented under NK2R-deficient conditions. Moreover, the antitumor effect of poly I:C treatment was abrogated by the absence of NK2R in vivo. Prior to this study, we confirmed that in vivo administration of poly I:C induced IFN-α and IFN-β production by $CD11c^+$ dendritic cells in the tumor microenvironment.[10] Previous papers have demonstrated that type I IFNs act directly on $CD8^+$ T cells to allow significant clonal expansion and to induce IFN-γ-producing effector cells in vivo.[39,40] Moreover, crucial roles of MDA5 and TLR3 have been indicated in poly I:C-mediated activation of antitumor effector NK cells accompanied by IFN-γ production.[41,42] In this study, we confirmed the involvement of NK cells in the antitumor effect of poly I:C treatment on the liver cancer-bearing model. These data suggest that IFN-α/β- or TLR3/MDA5-mediated IFN-γ productions by $CD8^+$ T cells or NK cells may contribute to the autocrine or paracrine NK2R expression of $CD8^+$ T cells in vivo. From these findings, we speculate that both type I and type II IFN–STAT1-mediated NK2R expression is involved in the induction of antitumor effector $CD8^+$ T cells in the tumor microenvironment to suppress the tumorigenesis of liver cancer cells in vivo. In this study, we could not confirm the effect of NK2R expression in $CD8^+$ T cells on antitumor immunity by adoptive transfer experiments transferring NK2R-deficient or sufficient $CD8^+$ T cells into immune-deficient mice. We will conduct these experiments in the near future.

HCC has a poor prognosis and is the most common primary liver cancer, accounting for ~90% of cases.[43] HCC can be treated by surgery, liver transplantation, chemotherapy, and liver-directed therapy; however, options for unresectable HCC are limited. Although some systemic drugs (atezolizumab plus bevacizumab, sorafenib, lenvatinib, regorafenib, cabozantinib, and ramucirumab) have been approved for advanced HCC, HCC is considered chemoresistant, and systemic chemotherapy is not routinely used.[12,44] In addition, patients with advanced HCC often have underlying liver disease, which is associated with poor tolerance to systemic chemotherapy. Therefore, for unresectable HCC patients, more effective treatments with fewer side effects are needed. Recently, several excellent therapeutic effects of immune checkpoint inhibitors in the standard treatment of HCC patients have been reported.[13,14] Our recent study revealed that DGKα blockade augmented antitumor effects in a liver cancer model, in which IFN-γ-producing $CD8^+$ T cells accumulated in tumor tissues in vivo.[20] Furthermore, we confirmed that DGKα blockade enhanced the antitumor efficacy of immune checkpoint inhibition therapy using an anti-PD-L1 antibody. On the basis of these findings, we speculated that IFN-γ production is a crucial event in the induction of antitumor immunity to eradicate liver cancer cells in the tumor microenvironment.

Taken together, we concluded that IFN-γ–STAT1-mediated NK2R expression is involved in the induction of antitumor effector $CD8^+$ T cells in a tumor microenvironment, which contributes to suppressing the tumorigenesis of cancer cells in vivo.

AUTHOR CONTRIBUTIONS

Conception and design: H. Kitamura. Development of methodology: W. Shen, X. Wang, H. Xiang, S. Shichi, H. Nakamoto, S. Kimura, K. Sugiyama, H. Kitamura. Acquisition of data (provided animals, acquired and managed patients, provided facilities, etc.): W. Shen, X. Wang, H. Xiang, S. Shichi, H. Nakamoto, S. Kimura, K. Sugiyama, H. Kitamura.

Analysis and interpretation of data (e.g., statistical analysis, biostatistics, computational analysis): W. Shen, X. Wang, H. Xiang, Taketomi, H. Kitamura. Writing, review, and/or revision of the manuscript: W. Shen, H. Kitamura. Administrative, technical, or material support (i.e., reporting or organizing data, constructing databases): A. Taketomi, H. Kitamura.

Study supervision: A. Taketomi, H. Kitamura.

ACKNOWLEDGMENTS

This work was partially supported by the Grant-in-Aid for Scientific Research (C) (22K07017 to H. Kitamura) from the Japan Society for the Promotion of Science (JSPS), the Japan Agency for Medical Research and Development (AMED) (22fk0310524h0001 to H. Kitamura and A. Taketomi), and the Joint Research Program of the Institute for Genetic Medicine, Hokkaido University (to A. Taketomi). We thank Melissa Crawford, PhD, from Edanz (https://jp.edanz.com/ac) for editing a draft of this manuscript. The content and data have been used as the thesis by Weidong Shen at Hokkaido University.

CONFLICT OF INTEREST STATEMENT

All authors declare no conflict of interest for this article.

ETHICS STATEMENT

N/A.INFORMED CONSENT: N/A.REGISTRY AND THE REGISTRATION NO. OF THE STUDY/TRIAL: N/A.ANIMAL STUDIES: All mouse experiments were approved by the Animal Ethics Committee of Hokkaido University (19–0036, 21–0026) and conducted in accordance with the recommendations in the Guide for the Care and Use of Laboratory Animals of the University.

ORCID

Hidemitsu Kitamura https://orcid.org/0000-0001-7006-6767

REFERENCES

1. O'Donnell JS, Teng MWL, Smyth MJ. Cancer immunoediting and resistance to T cell-based immunotherapy. *Nat Rev Clin Oncol*. 2019;16:151-167.
2. Waldman AD, Fritz JM, Lenardo MJ. A guide to cancer immunotherapy: from T cell basic science to clinical practice. *Nat Rev Immunol*. 2020;20:651-668.
3. Galon J, Bruni D. Approaches to treat immune hot, altered and cold tumours with combination immunotherapies. *Nat Rev Drug Discov*. 2019;18:197-218.
4. Munoz M, Rosso M, Covenas R. Neurokinin-1 receptor antagonists against Hepatoblastoma. *Cancers (Basel)*. 2019;11:1258.
5. Nizam E, Erin N. Differential consequences of neurokinin receptor 1 and 2 antagonists in metastatic breast carcinoma cells; effects independent of substance P. *Biomed Pharmacother*. 2018;108:263-270.
6. Severini C, Improta G, Falconieri-Erspamer G, Salvadori S, Erspamer V. The tachykinin peptide family. *Pharmacol Rev*. 2002;54:285-322.
7. Tuluc F, Lai JP, Kilpatrick LE, Evans DL, Douglas SD. Neurokinin 1 receptor isoforms and the control of innate immunity. *Trends Immunol*. 2009;30:271-276.
8. Kitamura H, Kobayashi M, Wakita D, Nishimura T. Neuropeptide signaling activates dendritic cell-mediated type 1 immune responses through Neurokinin-2 receptor. *J Immunol*. 2012;188:4200-4208.
9. Ohtake J, Kaneumi S, Tanino M, et al. Neuropeptide signaling through neurokinin-1 and neurokinin-2 receptors augments antigen presentation by human dendritic cells. *J Allergy Clin Immunol*. 2015;136:1690-1694.
10. Xiang H, Toyoshima Y, Shen W, et al. IFN-α/β-mediated NK2R expression is related to the malignancy of colon cancer cells. *Cancer Sci*. 2022;113:2513.
11. Ferlay J, Soerjomataram I, Dikshit R, et al. Cancer incidence and mortality worldwide: sources, methods and major patterns in GLOBOCAN 2012. *Int J Cancer*. 2015;136:E359-E386.
12. Kato A, Miyazaki M, Ambiru S, et al. Multidrug resistance gene (MDR-1) expression as a useful prognostic factor in patients with human hepatocellular carcinoma after surgical resection. *J Surg Oncol*. 2001;78:110-115.
13. Donisi C, Puzzoni M, Ziranu P, et al. Immune checkpoint inhibitors in the treatment of HCC. *Front Oncol*. 2020;10:601240.
14. Sangro B, Sarobe P, Hervas-Stubbs S, Melero I. Advances in immunotherapy for hepatocellular carcinoma. *Nat Rev Gastroenterol Hepatol*. 2021;18:525-543.
15. Byun CS, Hwang S, Woo SH, et al. Adipose tissue-derived mesenchymal stem cells suppress growth of Huh7 hepatocellular carcinoma cells via interferon (IFN)-beta-mediated JAK/STAT1 pathway in vitro. *Int J Med Sci*. 2020;17:609-619.
16. Zou J, Zhuang M, Yu X, et al. MYC inhibition increases PD-L1 expression induced by IFN-gamma in hepatocellular carcinoma cells. *Mol Immunol*. 2018;101:203-209.
17. Deng H, Kan A, Lyu N, et al. Tumor-derived lactate inhibit the efficacy of lenvatinib through regulating PD-L1 expression on neutrophil in hepatocellular carcinoma. *J Immunother Cancer*. 2021;9:e002305.
18. Deng R, Zuo C, Li Y, et al. The innate immune effector ISG12a promotes cancer immunity by suppressing the canonical Wnt/beta-catenin signaling pathway. *Cell Mol Immunol*. 2020;17:1163-1179.
19. Jin Y, Sun Z, Geng J, et al. IL-21 reinvigorates exhausted natural killer cells in patients with HBV-associated hepatocellular carcinoma in STAT1-depedent pathway. *Int Immunopharmacol*. 2019;70:1-8.
20. Okada N, Sugiyama K, Shichi S, et al. Combination therapy for hepatocellular carcinoma with diacylglycerol kinase alpha inhibition and anti-programmed cell death-1 ligand blockade. *Cancer Immunol Immunother*. 2022;71:889-903.
21. Toyoshima Y, Kitamura H, Xiang H, et al. IL6 modulates the immune status of the tumor microenvironment to facilitate metastatic colonization of colorectal cancer cells. *Cancer Immunol Res*. 2019;7:1944-1957.
22. Griebel G, Holsboer F. Neuropeptide receptor ligands as drugs for psychiatric diseases: the end of the beginning? *Nat Rev Drug Discov*. 2012;11:462-478.
23. Steinhoff MS, von Mentzer B, Geppetti P, Pothoulakis C, Bunnett NW. Tachykinins and their receptors: Contributions to physiological control and the mechanisms of disease. *Physiol Rev*. 2014;94:265-301.
24. Suvas S. Role of substance P neuropeptide in inflammation, wound healing, and tissue homeostasis. *J Immunol*. 2017;199:1543-1552.
25. Gleason NR, Gallos G, Zhang Y, Emala CW. Propofol preferentially relaxes neurokinin Receptor-2-induced airway smooth muscle contraction in Guinea pig trachea. *Anesthesiology*. 2010;112:1335-1344.
26. Mostafa GA, Reda SM, Abd El-Aziz MM, Ahmed SA. Sputum neurokinin a in Egyptian asthmatic children and adolescents: relation to exacerbation severity. *Allergy*. 2008;63:1244-1247.
27. Schelfhout V, Van De Velde V, Maggi C, Pauwels R, Joos G. The effect of the tachykinin NK2 receptor antagonist MEN11420 (nepadutant) on neurokinin A-induced bronchoconstriction in asthmatics. *Ther Adv Respir Dis*. 2009;3:219-226.
28. Sculptoreanu A, Aura Kullmann F, De Groat WC. Neurokinin 2 receptor-mediated activation of protein kinase C modulates capsaicin responses in DRG neurons from adult rats. *Eur J Neurosci*. 2008;27:3171-3181.
29. Sun J, Ramnath RD, Tamizhselvi R, Bhatia M. Neurokinin a engages neurokinin-1 receptor to induce NF-κB-dependent gene expression in murine macrophages: implications of ERK1/2 and PI 3-kinase/Akt pathways. *Am J Physiol Cell Physiol*. 2008;295:C679-C691.
30. Douglas SD, Leeman SE. Neurokinin-1 receptor: functional significance in the immune system in reference to selected infections and inflammation. *Ann N Y Acad Sci*. 2011;1217:83-95.
31. Eishingdrelo H, Kongsamut S. Minireview: targeting GPCR activated ERK pathways for drug discovery. *Curr Chem Genom Transl Med*. 2013;7:9-15.

32. Hauger RL, Olivares-Reyes JA, Dautzenberg FM, Lohr JB, Braun S, Oakley RH. Molecular and cell signaling targets for PTSD pathophysiology and pharmacotherapy. *Neuropharmacology*. 2012;62:705-714.
33. Zhang S, Lin X. CARMA3: scaffold protein involved in NF-κB signaling. *Front Immunol*. 2019;10:176.
34. Morelli AE, Sumpter TL, Rojas-Canales DM, et al. Neurokinin-1 receptor signaling is required for efficient Ca2+ flux in T-cell-receptor-activated T cells. *Cell Rep*. 2020;30:3448-3465.e3448.
35. Anfray C, Mainini F, Digifico E, et al. Intratumoral combination therapy with poly(I:C) and resiquimod synergistically triggers tumor-associated macrophages for effective systemic antitumoral immunity. *J Immunother Cancer*. 2021;9:e002408.
36. Dempoya J, Matsumiya T, Imaizumi T, et al. Double-stranded RNA induces biphasic STAT1 phosphorylation by both type I interferon (IFN)-dependent and type I IFN-independent pathways. *J Virol*. 2012;86:12760-12769.
37. Ohno Y, Toyoshima Y, Yurino H, et al. Lack of interleukin-6 in the tumor microenvironment augments type-1 immunity and increases the efficacy of cancer immunotherapy. *Cancer Sci*. 2017;108:1959-1966.
38. Wang Z, Chen T, Lin W, et al. Functional tumor specific CD8 + T cells in spleen express a high level of PD-1. *Int Immunopharmacol*. 2020;80:106242.
39. Kolumam GA, Thomas S, Thompson LJ, Sprent J, Murali-Krishna K. Type I interferons act directly on CD8 T cells to allow clonal expansion and memory formation in response to viral infection. *J Exp Med*. 2005;202:637-650.
40. Wiesel M, Crouse J, Bedenikovic G, Sutherland A, Joller N, Oxenius A. Type-I IFN drives the differentiation of short-lived effector CD8+ T cells in vivo. *Eur J Immunol*. 2012;42:320-329.
41. Miyake T, Kumagai Y, Kato H, et al. Poly I:C-induced activation of NK cells by CD8 alpha+ dendritic cells via the IPS-1 and TRIF-dependent pathways. *J Immunol*. 2009;183:2522-2528.
42. McCartney S, Vermi W, Gilfillan S, et al. Distinct and complementary functions of MDA5 and TLR3 in poly(I:C)-mediated activation of mouse NK cells. *J Exp Med*. 2009;206:2967-2976.
43. Llovet JM, Kelley RK, Villanueva A, et al. Hepatocellular carcinoma. *Nat Rev Dis Primers*. 2021;7:7.
44. Jiang W, Lu Z, He Y, Diasio RB. Dihydropyrimidine dehydrogenase activity in hepatocellular carcinoma: implication in 5-fluorouracil-based chemotherapy. *Clin Cancer Res*. 1997;3:395-399.

SUPPORTING INFORMATION

Additional supporting information can be found online in the Supporting Information section at the end of this article.

How to cite this article: Shen W, Wang X, Xiang H, et al. IFN-γ–STAT1-mediated NK2R expression is involved in the induction of antitumor effector $CD8^+$ T cells in vivo. *Cancer Sci*. 2023;114:1816-1829. doi:10.1111/cas.15738